AMERICAN JOURNAL OF BIOCHEMISTRY AND BIOTECHNOLOGY

RESEARCH ARTICLE

Detection of Exogenous Heavy Metal Pesticide Residues in Traditional Chinese Medicine Based on Fluorescent Carbon Quantum Dots

Yanan He, Shuyin Wang*

Department of Pharmacy, Cangzhou Medical College, Cangzhou 061000, China

*Corresponding Author: wsy0400120@126.com

Abstract: The analysis method based on fluorescent probes has received increasing attention due to its high sensitivity, fast response, and real-time visualization characteristics. Therefore, the application of fluorescent probes for rapid detection of heavy metal pesticide residues in traditional Chinese medicine is of great significance. This study innovatively synthesized B/N co-doped carbon quantum dots using 3-aminophenylboronic acid as the raw material, and based on this, constructed a ratio fluorescent probe for detecting Cr6+ in traditional Chinese medicine. The results showed that the concentration of Cr6+ exhibited a good linear relationship within the concentration range of 0 to 100 μmol•L-1, with an R2 of 0.999. The detection limit of the research method for Cr6+ in traditional Chinese medicine was 0.39 μmol•L-1, and the recovery rate fluctuated within the range of 89.3% - 111.7%. In actual sample testing, the Cr6+ content in Panax ginseng and Salvia miltiorrhiza was 0.0311 g•kg-1 and 0.0186 g•kg-1, respectively. These results fully demonstrate the effectiveness and practicality of B/N co-doped carbon quantum dot fluorescent probes in the detection of Cr6+ in traditional Chinese medicine.

Keywords: Fluorescent Carbon Quantum Dots, Traditional Chinese Medicine Hexavalent Chromium, Boron/nitrogen Co-Doping, Hydrothermal Method

Received: 14-04-2025 | **Revised:** 14-04-2025 | **Accepted:** 29-05-2025 | **DOI:** 10.3844/ajbbsp.2026.22.01.008

Introduction

Chinese Medicinal Herbs (CMHs), as an indispensable part of traditional medicine, play an indispensable role in treating diseases and maintaining health. However, with the increasingly serious problem of environmental pollution, the issue of exogenous heavy metal pesticide residues in Traditional Chinese Medicine (TCM) has gradually become a focus of public attention. Among these exogenous pollutants, heavy metals have attracted much attention due to their potential health risks. Their presence not only significantly weakens the efficacy of TCM, but also poses a potential threat to human health [1, 2]. To ensure the safety and efficacy of TCM, various analytical techniques have been taken for detecting exogenous heavy metal pesticide residues in TCM. For example, Shuo et al. proposed a multi-channel visual array sensor built on nitrogen (N)-doped CO dots and gold nanoclusters to achieve precise detection of various metal ions in tap water, soil, and TCM. The detection limits for cadmium (Cd2+), lead (Pb2+), and mercury (Hg2+) in this method were 0.15, 0.20, and 0.09 (μmol/L) [3]. Rui et al.

used Monte Carlo simulation to determine the levels of heavy metal pollution in 90 batches of verbascos flowers to assess the non-carcinogenic and carcinogenic risks caused by heavy metal accumulation. The arsenic (As) element in hairy flowers was the main factor causing non-carcinogenic and carcinogenic risks [4]. Yu et al. proposed an ion imprinted electrochemical sensor grounded on nanomaterials to design a fast and convenient method for detecting heavy metal ions. The electrode surface modified with nanomaterials has achieved excellent nano effects, greatly improving its surface area and conductivity, thereby enhancing the sensitivity of the sensor for heavy metal detection and reducing the detection limit of the sensor [5].

The development of technology and the deepening of research have brought Fluorescent Carbon Quantum Dot (FCQD) technology into the public eye. This technology can quantitatively analyze the content of pollutants in samples through changes in Fluorescence Intensity (FluI). It is not only easy to operate, but also has a fast response speed, making it very suitable for rapid on-site detection [6, 7]. In addition, the surface of Carbon Quantum Dots (CQDs) can be functionalized to enhance their binding ability with specific pollutants, thereby greatly improving the selectivity and sensitivity of detection [8]. Therefore, numerous researchers have explored FCQD technology. For example, Lv et al. modified lignin using sulfamethoxazole, p-ABSA, and ammonium aminosulfonate as amination reagents to endow CQDs with special functions. A sulfonamide lignin composite CQDs (PSA-L-CQDs) was prepared using citric acid as the raw material, and the selectivity of PSA-L-CQDs to metal ions were measured by fluorescence spectroscopy. PSA-L-CQDs exhibited high sensitivity towards iron (Fe^{3+}). The detection constrains of Fe^{3+} was 29.5634 nmol/L [9]. Shen and He et al. prepared a stable and non-toxic FCQD using natural bark tannins as raw materials via hydrothermal method. After incubating human embryonic alveolar epithelial cells in high concentration FCQD at 200 mg/L for 24 hours, the cell survival rate kept as 90%, and clear fluorescence images could be found under laser confocal fluorescence microscopy [10]. Katakami et al. synthesized a red FCQD using 4, 6- diaminoresorcinol dihydrochloride (DAR). The surface of FCQDs derived from DAR contains hydroxyl and amino groups, which can promote fluorescence quenching of metal ions like aluminum (Al^{3+}), Fe^{3+}, copper (Cu^{2+}), and lead (Pb^{2+}) [11].

In summary, there are currently numerous methods for heavy metal detection, each with its own advantages. Among them, FCQD, as a novel fluorescent nanomaterial, has received widespread attention due to its unique optical properties and low toxicity. Compared with traditional quantum dots, CQDs have better biocompatibility and environmental friendliness, making them show great potential in the field of biomedical detection. In the detection of exogenous pollutants in TCM, CQDs can be used as fluorescent probes to achieve high-sensitivity detection of these pollutants by specific binding with heavy metal ions or pesticide molecules. However, there are relatively few reports on the detection technology based on FCQD in the field of TCM. In addition, although the 2020 edition of the *Chinese Pharmacopoeia* has set clear limit standards for heavy metals such as Cd^{2+}, Pb^{2+}, Cu^{2+}, Hg^{2+}, and As, the limit regulations for other heavy metals such as nickel (Ni^{2+}), manganese (Mn^{2+}), hexavalent chromium (Cr^{6+}), and barium (Ba^{2+}) are not yet clear. This may become a hidden danger in the quality supervision of heavy metals in TCM. Therefore, based on previous research, this study innovatively uses 3-aminophenylboronic acid as the synthetic raw material and prepares CQDs doped with boron (B) and N elements by hydrothermal method. A ratio sensing platform for detecting exogenous Cr^{6+} pesticide residues in TCM is designed using the fluorescence dual photoluminescence characteristics of B/N co-doped CQDs (B/N-CQD). This method aims to provide more reliable technical support for the quality control of TCM. Meanwhile, this study also aims to fill the gap in the *Chinese Pharmacopoeia* regarding the missing limit standards for Cr^{6+}, and promote the comprehensive improvement of the safety of TCM materials.

Cr^{6+} and Its Hazards

Chromium mainly exists in two valence states in nature, namely trivalent chromium (Cr^{3+}) and Cr^{6+} [12]. Among them, Cr^{3+} can regulate glucose and lipid metabolism in the human body, which is beneficial to health [13]. Cr^{6+} is the main toxic form of chromium in industrial production and a common heavy metal pollutant. The specific forms of harm of Cr^{6+} to the human body are shown in Figure 1.

DOI: 10.3844/ajbbsp.2026.22.01.008

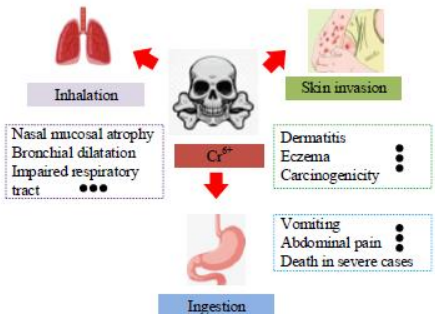

Fig. 1: Specific forms of Cr^{6+} harm to humans

In Figure 1, Cr^{6+} is a highly mutagenic substance that can enter the human body through skin contact and inhalation, thereby inducing lung cancer and nasopharyngeal cancer [14]. It is easily absorbed by the human body and accumulates in the body, posing a serious threat to human health. Therefore, strict control of Cr^{6+} pollution is crucial. However, economic development and changes in the ecological environment have had varying degrees of impact on the quality of TCM. For example, the application of Cr^{6+} in industries such as ore smelting and leather processing, if not properly discharged, can accumulate in the environment, causing 3 water and soil pollution, leading to passive absorption by medicinal plants during their growth process, resulting in excessive Cr^{6+} content in TCM. In addition, the absorption and enrichment of Cr^{6+} by different medicinal parts of TCM also vary, which can lead to different degrees of pollution [15]. For example, the Cr^{6+} content of root and stem medicinal herbs such as Panax ginseng and Salvia miltiorrhiza is usually higher than that of Artemisia argyi. It is worth noting that during the collection, transportation, processing, and processing of TCM, Cr^{6+} contamination may also be introduced through containers or excipients. Therefore, building a dynamic monitoring network for Cr^{6+} concentration is of great significance in providing support for preventing and controlling Cr^{6+} pollution and reducing the risk of Cr^{6+} enrichment in TCM and human body.

Materials and Methods

Main Instruments and Equipment

Table 1: Lists the main reagents required for this study.

Table 1: Main reagents

Reagent name	Chemical formula	Fineness	Manufacturer
Potassium dichromate standard solution	K2Cr2O7	Analyzed pure	Macklin
Nitric acid	HNO3	Analyzed pure	Macklin
Perchloric acid	HClO4	Analyzed pure	Macklin
3-Aminophenylboronic acid	C6H7BNO2	Analyzed pure	Macklin
Quinine Sulfate	C20H24N2O2·H2S O4	Analyzed pure	Macklin
Fluorescein	C20H12O5	Analyzed pure	Aladdin
Hydroxyethylpiperazine ethanesulfonic acid (HEPES)	C8H18N2O4S	Analyzed pure	Aladdin
Carmine	C20H11N3Na2O7 S3.2H2O	Analyzed pure	Aladdin
Ethylenediaminetetraacetic acid disodium salt	C10H12N2Na2O8	Analyzed pure	Aladdin
Alizarin Red Sodium Salt	C22H11Na2O7S	Analyzed pure	Aladdin
Mercury nitrate standard solution	Hg (NO3)2	Analyzed pure	Aladdin
Magnesium Chloride	MgCl2	Analyzed pure	Aladdin
Deuterated dimethyl	(CD3)2SO	Analyzed pure	Aladdin
Sulfoxide (DMS O-d6)			

DOI: 10.3844/ajbbsp.2026.22.01.008

Table 2 shows the main instruments and equipment to be used.

Table 2: Main instrumentation

Instruments and equipment	Model number	Manufacturer
X-ray Photoelectron Spectroscopy (XPS)	Ultra DLD	Kratos Analytical
Transmission Electron Microscopy (TEM)	FEI Tecnai G2 F20	Thermo Fisher Scientific
Fourier Infrared Spectroscopy (FT-IR)	Bruker Vertex 70	Bruker Optics
Mass Spectrometer (MS)	Agilent 5977B	Agilent Technologies
Nuclear Magnetic Resonance Spectrometer (NMR)	Varian VNMRS 600	Thermo Fisher Scientific
Ultraviolet-Visible Spectrophotometer (UV-VIS)	UV-2600	Shimadzu Corporation
Fluorescence Spectrophotometer (FL)	LS 55	PerkinElmer
Fully Automated Fluorescence Lifetime Spectrometer	FLS 980	Edinburgh Instruments
Inductively Coupled Plasma Emission Spectrometer (ICP-OES)	iCAP 6300	Thermo Fisher Scientific

The reagents used in the experiment are used directly without purification treatment. The TCM materials used in the experiment are shown in Figure 2.

Fig. 2: Chinese herbal medicine

In Figure 2, this study uses Panax ginseng and Salvia miliotrhiza as research subjects, both of which are purchased from a medicinal herb market in Sichuan Province.

Experimental Methods

Preparation of B/N-CQD

The specific preparation process of B/N-CQD is shown in Figure 3.

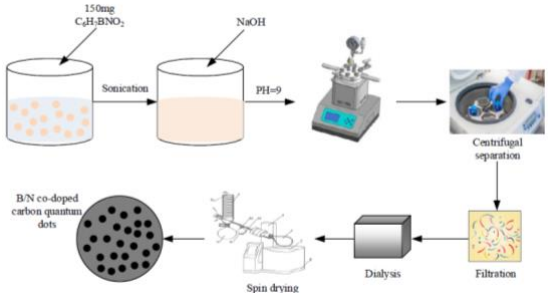

Fig. 3: Process for the preparation of B/N-CQD

In Figure 3, at room temperature, this study first accurately weighed 150 mg of C6H7BNO2 and then placed it in 50 ml of deionized water. After 5 minutes of ultrasonic treatment to fully dissolve it, a 0.1 mol·L-1 NaOH solution was slowly dropped and the pH of the solution was adjusted to 9.0. After pH adjustment, the solution was transferred to a 100 mL stainless steel

DOI: 10.3844/ajbbsp.2026.22.01.008

high-pressure reactor lined with Teflon and reacted at temperatures of 150℃, 170℃, 190℃, and 210℃ for 6 hours. After the reaction was completed, the reaction kettle was taken out and left to cool and centrifuge at room temperature. The supernatant was filtered through a 0.22 μm microporous membrane, and then the filtrate was transferred to a dialysis bag for 24 hours to obtain a uniform B/N-CQD solution. Finally, the solution was subjected to rotary evaporation drying and redispersed according to different concentrations for subsequent experimental use.

Characterization Testing and Spectral Analysis Methods

This study mainly used TEM to observe the morphology, PSD, and lattice spacing of B/N-CQD. The elemental composition and surface functional groups of B/N-CQD were investigated through FT-IR and XPS analysis, and structural information about B/N-CQD was collected using NMR and MS techniques. In addition, the optical characteristics of these CQDs were analyzed using UV-VIS and FL. These characterization testing methods can provide a solid foundation for a comprehensive understanding of the physical and chemical properties of B/N-CQD. The experiment used C20H24N2O2·H2SO4 (360 nm) and C20H12O5 (490 nm) as reference materials. The quantum yield calculation formula for B/N-CQD is shown in Equation (1):

$$\phi_u = \phi_s \times \frac{F_u \times A_s \times n^2{}_u}{F_s \times A_u \times n^2{}_s} \quad (1)$$

In Equation (1) $\phi_u / \phi_s, F_u / F_s, A_u / A_s, and\, n_u / n_s$ represent the fluorescence quantum yield, fluorescence emission peak area integral, absorbance at excitation wavelength, and solvent refractive index of B/N-CQD with a reference substance.

This study investigated the fluorescence response of B/N-CQD to various concentrations of Cr6+ by adding a series of Cr6+ ions to the B/N-CQD solution at excitation wavelengths of 360nm and 490nm. To assess the B/N-CQD selectivity towards Cr6+, this study also added 200 μmol·L-1 Cr2O72- and various interfering ions to the B/N-CQD solution, and recorded the fluorescence emission spectra at the same excitation wavelength. At the same time, to test the fluorescence response of B/N-CQD to Cr6+ in the existence of Fe3+ and Hg2+, 200 μmol·L-1 EDTA was added as a masking agent in the experiment, and the fluorescence changes were recorded. To further verify the anti-interference ability of B/N-CQD on Cr6+, this study reduced the concentration of Cr2O72- to 100 μmol·L-1 and adjusted the concentration of other interfering ions to 2 mmol·L-1. In solutions containing Cr3+, Al3+, Cu2+, Fe2+, and Fe3+, the concentration of EDTA was set to 2 mmol·L-1, while in Hg2+ solution, the concentration of EDTA increased to 4 mmol·L-1. In addition, to investigate the internal filtration effect of B/N-CQD, this study also recorded the UV visible absorption spectra of Cr6+ (200 μmol·L-1), carmine (30 μmol·L-1), and ARS (100 μmol·L-1). In the presence of these substances, the three-dimensional fluorescence spectra of B/N-CQD solution were measured. These spectral analysis steps aim to comprehensively evaluate the detection performance and selectivity of B/N-CQD for Cr6+in complex environments.

All the above experiments were conducted in a 10 mmol·L-1 HEPES buffer solution (pH = 7.5) with a B/N-CQD solution concentration of 0.06 mg·mL-1. The response mechanism of B/N-CQD to Cr6+ is shown in Figure 4.

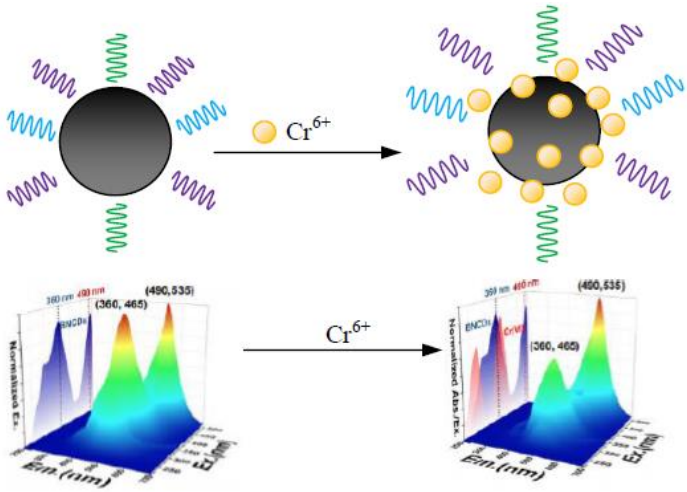

Fig. 4: Response mechanism of B/N-CQD to Cr6+

In Figure 4, the B/N-CQD's fluorescence properties change when Cr6+ is present. Cr6+, as a heavy metal ion, can interact with functional groups in show of B/N-CQD or with the electronic structure of B/N-CQD through IFE, resulting in a decrease or quenching of FluI. This change in FluI can be used to detect the presence of Cr6+ and quantitatively analyze its concentration.

Collection and Preparation of Actual Samples

The lake water specimen was collected from the campus of Chengdu University of Technology and filtered through a 0.22 μm microporous membrane to remove particulate matter. Then, HEPES buffer was added to adjust the pH to 7.5 for future use. The soil samples were collected from a factory in Sichuan Province that involved chrome plating technology. They were pre-treated according to the US Environmental Protection Agency's 3060 A method, first drying the soil samples and thoroughly grinding them using a mortar. Next, dissolve 20.0 g NaOH and 30.0 g Na2CO3 in deionized water to prepare a 100 ml digestion solution. Take 1.25 g of soil fine powder into a digestion container, add 25 ml of digestion solution, 200 mg of MgCl2, and 0.25 ml of 1.0 mol·L-1 HEPES buffer solution. After stirring at room temperature for 10 min, the container was transferred to a water bath and stirred for 1 h at 95℃. After cooling to room temperature, centrifugation was performed, and the supernatant was filtered through a 0.22 μm filter membrane. Under continuous stirring, add 5.0 mol·L-1 nitric acid solution dropwise to the filtered supernatant and adjust the pH of the filtrate to 5.5. Subsequently, the solution was sonicated for 30 minutes to remove CO2, and the pH was adjusted to 7.5. The processed solution was quantitatively transferred to a 50 ml volumetric flask and diluted to the mark with deionized water. After shaking well, it was set aside for later use.

The sample processing of CMHss Panax ginseng and Salvia miltiorrhizia follows the methods described in the 2020 edition of the Chinese Pharmacopoeia [16, 17]. Firstly, after the medicinal herbs are crushed, 1 g of coarse powder is taken, accurately weighed, and placed into a 50 ml conical flask. Then, 10 ml of a digestion solution prepared in a 4:1 volume ratio of nitric acid and perchloric acid is added, mixed well, and soaked overnight. The next day, the conical flask was placed on an electric heating plate and heated for digestion in a slightly boiling state. If the color of the solution darkens to brownish black, an appropriate amount of digestion solution can be added and heated until the solution becomes clear and transparent. Then increase the temperature until the white smoke dissipates and the digestion solution evaporates completely. The residue was dissolved in 10 ml of 1.0 mol·L-1 HEPES buffer (pH = 7.5). After centrifugation and filtration, the filtrate obtained is used for subsequent analysis [18, 19].

For all actual samples, this study used a B/N-CQD based method for spiked recovery experiments, by adding different concentrations of Cr6+ and 200 μmol·L-1 EDTA for sample determination. The recovery rate of spiked samples is calculated using the linear regression equation obtained from standard experiments to evaluate the accuracy and reliability of the research method.

Preparation of Fluorescent Test Strips

This study first soaked non fluorescent cellulose filter paper in a 0.4 mg·mL^{-1} B/N-CQD aqueous solution for 5 minutes, and then dried it in a vacuum drying oven at 60℃ for 2 hours. The dried test strips were rapidly immersed in Cr^{6+} aqueous solutions of different concentrations, with concentrations of 2, 20, 200, and 2000, respectively in units of μmol·L^{-1}. The soaking time for each concentration is 5 seconds. The soaked test paper is taken out and naturally dried. Finally, fluorescence images of the test strips at excitation wavelengths of 360 nm and 490 nm were captured using a smartphone to record their fluorescence response.

Experimental Results

Exploration and Characterization Analysis of the Optimal Preparation Temperature for B/N-CQD

The reaction temperature is a key factor affecting the properties of B/N-CQD. By adjusting the reaction temperature, the size and morphology of B/N-CQD can be controlled, thereby affecting its optical properties. To investigate the influence of temperature on the fluorescence characteristics of B/N-CQD, this study conducted emission spectroscopy tests on B/N-CQD synthesized at different reaction temperatures under excitation wavelengths of 360 nm and 490 nm. The test results are shown in Figure 5.

DOI: 10.3844/ajbbsp.2026.22.01.008

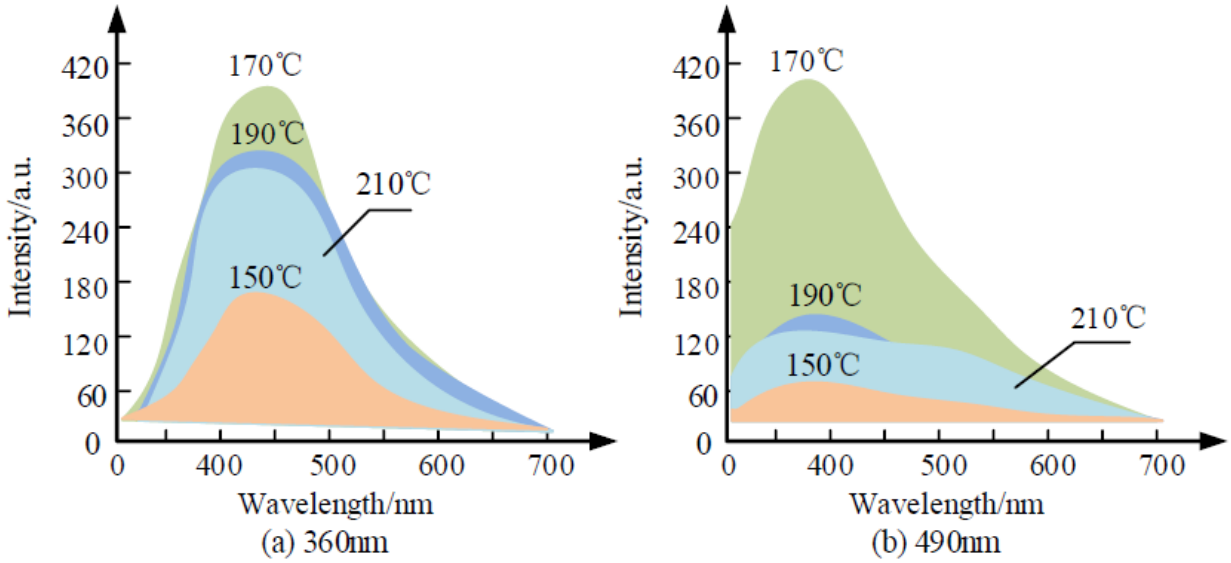

Fig. 5: Fluorescence spectra of B/N-CQD under different conditions

Figures 5 (a) and (b) show the B/N-CQD fluorescence spectra synthesized at different temperatures under excitation wavelengths of 360 nm and 490 nm. Whether at an excitation wavelength of 360 nm or 490 nm, the FluI of B/N-CQD increases as the temperature increases from 150℃ to 170℃. However, as the temperature continues to rise, its FluI shows a decreasing trend. Excessive temperature can lead to an increase in surface defects or changes in energy level structure of quantum dots, thereby affecting their fluorescence performance. Therefore, to obtain the best fluorescence characteristics, 170℃ is chosen as the optimal preparation temperature for B/N-CQD in this study. At this temperature, the size, morphology, and optical properties of quantum dots can reach an equilibrium state, which is beneficial for their application in fluorescent probes. The morphology and PSD of B/N-CQD synthesized at 170℃ are shown in Figure 6.

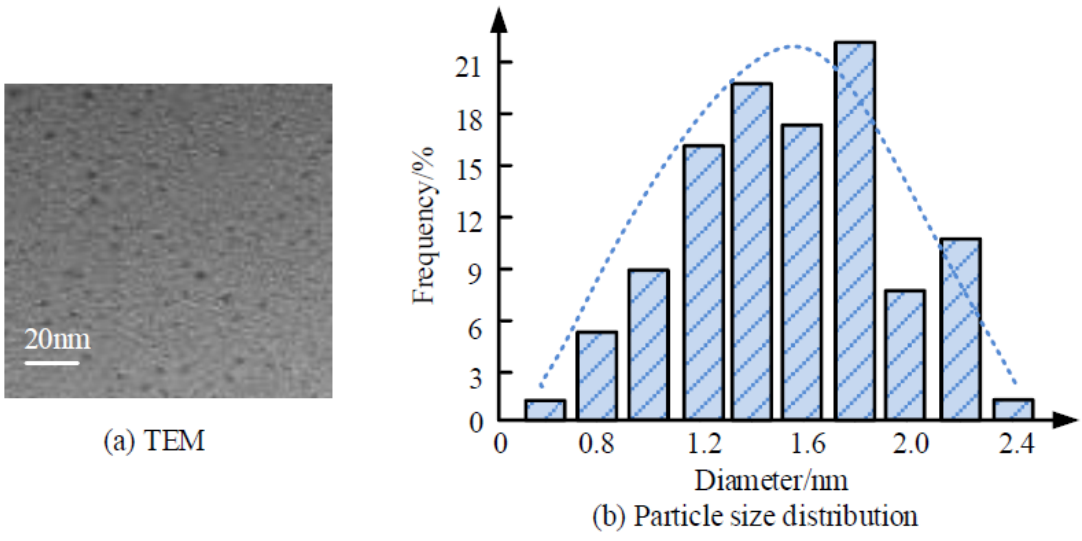

Fig. 6: Morphological features and PSD of B/N-CQD

Figures 6 (a) and (b) show the morphological characteristics and PSD of B/N-CQD synthesized at 170℃. In Figure 6 (a), the B/N-CQD prepared at 170℃ has a regular spherical appearance and is evenly distributed in the field of view without obvious agglomeration. This uniform distribution helps ensure the consistency and reliability of B/N-CQD in the application

process. In Figure 6 (b), the particle size of B/N-CQD is mainly concentrated in the range of 0.5 nm-2.4 nm, with an average particle size of 1.6 nm. This PSD range is ideal for CQDs, as they typically exhibit strong fluorescence emission and good biocompatibility within this size range. In addition, smaller and uniform PSD makes it easier to penetrate cell membranes and reduces potential toxicity to biological systems. Under the synthesis conditions of 170, the morphology and Particle Size Distribution (PSD) of B/N-CQD can exhibit good characteristics.

The Optimal Experimental Parameter Settings for B/N-CQD and the Detection Effect of Cr_{6+}

This study first investigated the concentration and pH parameters of B/N-CQD prepared under synthesis conditions at 170℃ to determine the optimal experimental parameters, as shown in Figure 7.

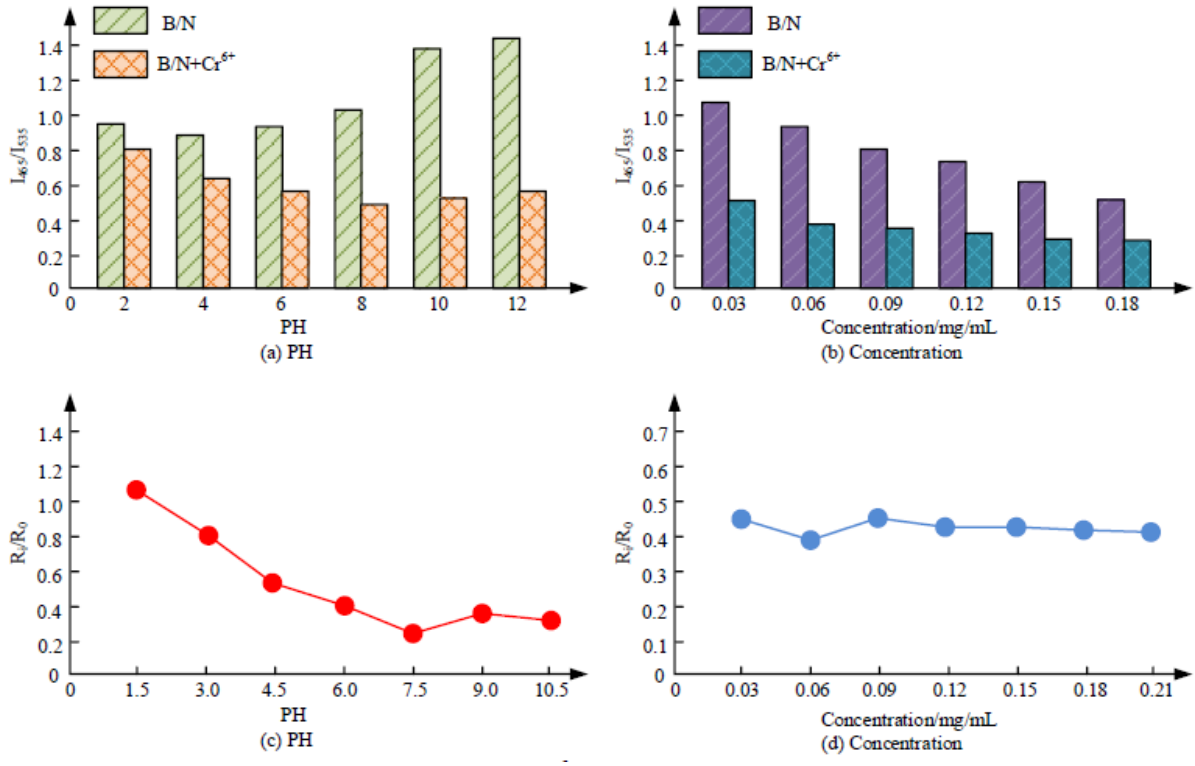

Fig. 7: Concentration effect and PH effect of B/N-CQD in Cr_{6+} ratio detection

Figures 7 (a)/(c) and (b)/(d) show the pH and concentration effects of B/N-CQD in Cr_{6+} ratio detection. In Figures 7 (a) and (c), as the pH value rises, the FluI ratio of B/N-CQD shows a significant decreasing trend between pH 2 and pH 7.5. This indicates that Cr_{6+} has a strong Fluorescence Quenching Effect (FQE) on B/N-CQD within this pH range. The FluI ratio of B/N-CQD shows a slow increasing trend between pH 7.5 and pH 10, indicating that this pH range has a weak effect on the FQE. At pH 7.5, the FluI ratio reaches its lowest point and exhibits the strongest FQE. In Figures 7 (b) and (d), as the concentration of B/N-CQD increases, the FluI ratio also increases. However, after the B/N-CQD concentration reaches 0.06 mg/mL, the increasing trend will become gentle. When the concentration of B/N-CQD is 0.06 mg/mL, the detection sensitivity of B/N-CQD for Cr_{6+} is high. Taking into account the FluI, detection sensitivity, and ease of experimental operation, this study ultimately chose a B/N-CQD concentration of 0.06 $mg \cdot mL^{-1}$ and pH=7.5 as the optimal experimental conditions. Under these experimental conditions, this study tested the detection effect of Cr_{6+} in B/N-CQD through titration experiments, as shown in Figure 8.

DOI: 10.3844/ajbbsp.2026.22.01.008

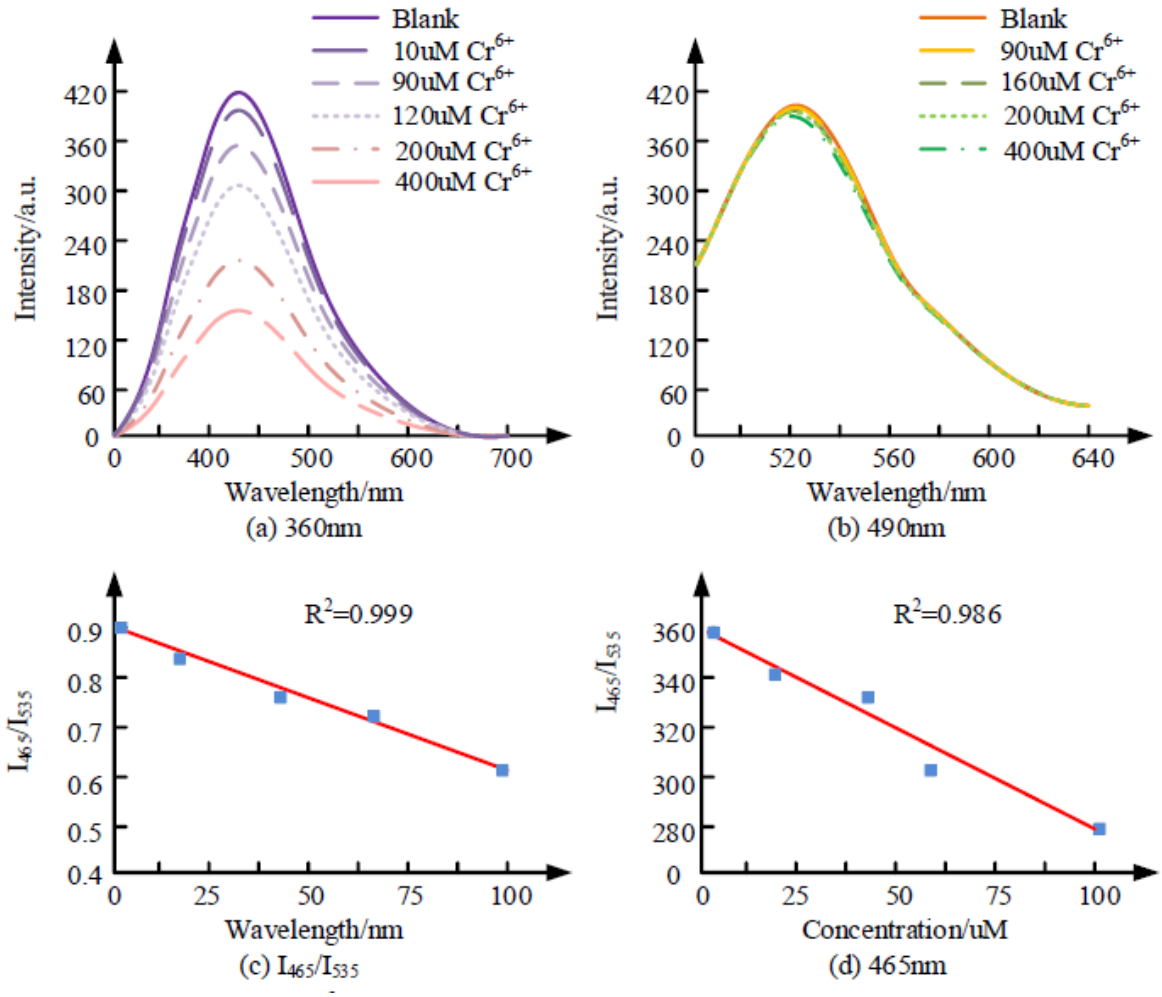

Fig. 8: Results of fluorescence response of Cr^{6+} at different excitation wavelengths

Figures 8 (a) and (b) show the fluorescence response results of Cr6+ at different concentrations under excitation wavelengths of 360 nm and 490 nm. Figures 8 (c) and (d) show the linear fitting results of B/N-CQD at I465/I535 ratio and 465 nm excitation wavelength. When the excitation wavelength is 360nm, as the concentration of Cr6+ gradually grows, the fluorescence emission intensity of B/N-CQD at 465 nm gradually decreases. However, when the excitation wavelength is 490 nm, no significant fluorescence quenching phenomenon occurs in B/N-CQD with the gradual increase of Cr6+ concentration. By measuring the relationship between the emission intensity ratio (I465/I535) of B/N-CQD and the concentration of Cr6+ within the range of 0-100 μmol·L-1, a linear regression curve with a determination coefficient of 0.999 is obtained. This result is superior to the R2 value (0.986) based solely on the FluI change at 465 nm. In addition, according to the calculation of 3 times the standard deviation of the blank solution, the detection limit of the research method for Cr6+ is 0.39 μmol·L-1, which is much lower than the max allowable concentration of Cr6+ in the national wastewater discharge standard of 0.5 mg/L. Therefore, B/N-CQD has high sensitivity and accuracy in Cr6+ detection.

Detection of Exogenous Cr^{6+} Residual Pollutants

This study quantitatively analyzed Cr^{6+} in soil samples, lake water samples, and TCM samples using a ratio fluorescence sensor based on B/N-CQD. The study tries to ensure the accuracy of the detection method. Table 3 lists the spiked recovery experimental data for evaluating the performance of the sensor.

DOI: 10.3844/ajbbsp.2026.22.01.008

Table 3: Spiked recovery of Cr6+ in real samples (n = 3)

Samples	Cr6+addition /μmol·L-1	Cr6 + measured value/μmo l·L-1	Recovery rate /%	RSD/%	Quantity contained/ g·Kg-1
Lake	0	0	/	/	/
30	26.8	89.3	0. 3		/
60	54.6	91.0	1. 0		/
90	85.6	95.1	0. 3		/
Soils	0	0	/	/	/
30	28.8	96.0	0. 6		/
60	70.0	111.7	0. 6		/
90	97.5	109.4	0. 7		/
Panax ginseng	0	29.6	/	/	0.0311
30	61.6	107.7	0. 4		/
60	86.8		95.8		0. 3
90	112.4		92.3		0. 2
Salvia miltiorrhiza	0	18.4	/	/	0.0186
30	49.8		105.7		1. 1
60	76.1		96.7		1. 2
90	106.3		98.0		0. 6

In Table 3, no presence of Cr6+ is found in the analysis of lake water and soil samples. Cr6+ content of 0.0311g·kg-1 and 0.0186g·kg-1 are detected in two TCM materials, Panax ginseng and Salvia miltiorroza, respectively. By comparing the experimentally measured Cr6+ concentration with pre-added Cr6+ standard concentrations of 30, 60, and 90 μmol·L-1, it is found that the recovery rate of the research method fluctuated within the range of 89.3%-111.7%. This validates the effectiveness and accuracy of using B/N-CQD as a sensor to detect Cr6+ in actual sample analysis. At the end of this study, other FCQD methods are also introduced for comparative experiments, as displayed in Table 4.

Table 4: Detection results of different FCQD methods

Transducers	Grain size/nm	Linear range/μmol·L-1	Detection limit/μmol·L-1	Ref.
PSA-L-CQDs	6.40	0-140	40	[9]
DAR	3.02	10-100	1.25	[11]
GQDs	1.20	0.05-500	3.7	[16]
DECDs	3.20	2-300	0.4	[17]
CCDs	2.93	5-125	1.17	[18]
PNCQDs	5.14	1.5-30	23	[19]
Research method	1.60	0-100	0.39	Current Study

In Table 4, compared to other FCQD techniques, the B/N-CQD fluorescence detection method exhibits significant advantages in sensitivity and accuracy. The experiment further confirms the potential application of B/N-CQD in detecting Cr_{6+} in actual samples.

Conclusion

TCM plays a unique role in disease prevention and treatment, making significant contributions to social development and medical civilization progress. Its products are becoming increasingly popular worldwide. However, safety issues such as excessive Cr_{6+} content caused by TCM cultivation and processing seriously hinder the globalization of TCM. In view of this, this study proposed a novel B/N-CQD ratio sensing platform for detecting exogenous Cr_{6+} pesticide residues in TCM, utilizing the fluorescence dual photoluminescence characteristics of B/N-CQD. By optimizing the experimental conditions, this study determined that the optimal temperature for preparing B/N-CQD was 170℃, the optimal concentration was 0.06 mg·L_{-1}, and

pH was 7.5. Under the optimal experimental preparation conditions, this study conducted a series of analytical tests. Actual sample testing showed that the detection limit of the research method for Cr^{6+} was 0.39 μmol·L^{-1}, which was much lower than the maximum allowable concentration of Cr^{6+} in the national wastewater discharge standard of 0.5 mg·L^{-1}. Cr^{6+} content of 0.0311 g·kg^{-1} and 0.0186 g·kg^{-1} were detected in two TCM materials, Panax ginseng and Salvia miltiorroza, respectively. In addition, compared with other FCQD technologies, the research method performs the best. Although significant achievements have been made in the detection of Cr^{6+} in TCM in this study, there is still room for further expansion. Future research can explore the application of this sensing platform in other types of TCM and different environmental samples, in order to provide more comprehensive support for the safety assessment and global development of TCM.

Acknowledgment

Thank you to the publisher for their support in the publication of this research article. We are grateful for the resources and platform provided by the publisher, which have enabled us to share our findings with a wider audience. We appreciate the efforts of the editorial team in reviewing and editing our work, and we are thankful for the opportunity to contribute to the field of research through this publication.

Funding Information

The author received no specific funding for this work.

Author's Contributions

Both the authors have equally contributed to this manuscript.

Ethics

This article is original and contains unpublished material. The corresponding author confirms that all of the other authors have read and approved the manuscript and no ethical issues involved.

Conflict of Interest

The authors declare that they have no competing interests.

Data Availability Statement

The data used to support the findings of this study are all in the manuscript.

References

1. Sheng YG, Tian TZ, Zhen AC. Progress in quality control, detection techniques, speciation and risk assessment of heavy metals in marine traditional Chinese medicine. *Chin Med.* 2023;18(1):73–75.
2. Li M, Ji H, Liu Y. Association between heavy metal exposure and height in Chinese preschoolers. *J Occup Environ Med.* 2023;65(7):567–572.
3. Shuo W, Gaoqiong D, Jian Y. Carbon dot and gold nanocluster-based three-channel fluorescence array sensor for visual detection of multiple metal ions. *Sens Actuators B Chem.* 2022;358:131xxx. *(verify article number/pages)*
4. Rui H, Shaowei C, Ping W. Heavy metals and probabilistic risk assessment via *Prunella vulgaris* consumption in Guangdong Province, China. *Toxicol Res.* 2024;13(5):xxx–xxx. *(verify volume/pages)*
5. Yu L, Sun L, Zhang Q, Zhou Y, Zhang J, Yang B, et al. Nanomaterials-based ion-imprinted electrochemical sensors for heavy metal ion detection: a review. *Biosensors.* 2022;12(12):1096.
6. Rana AS, Negi P, Rawat BS, Joshi NC, Upadhyay S, Kumar N, et al. Synthesis of nitrogen-doped carbon quantum dots from *Dieffenbachia seguine* leaves for fluorescent pH sensing. *Asian J Chem.* 2023;35(3):727–731.
7. Jenitha RF, Sudhaparimala S. Microwave conversion of *Plantago psyllium* husk into carbon quantum dots for sensing heavy metals and removal of organic dyes. *Indian J Chem Technol.* 2023;30(6):863–871.
8. Moustafa AH, Mousa MA, Abdelrahman HH, Fahmy MA, Ebrahim DG. Detection of antibiotics and heavy metals using fluorescence silver/graphene quantum dots nanocomposites. *Appl Nanosci.* 2024;14(1):1–20.

9. Lv S, Zhang S, Zuo J. Detection of Fe^{3+} using sulfonamidated lignin composite carbon quantum dots. *Polym Eng Sci.* 2023;63(5):1439–1447.
10. Shen J, He Z. Tannin-derived carbon quantum dots for detection of Cr^{6+} ions, bioimaging, and fluorescent ink applications. *Ind Eng Chem Res.* 2023;62(8):3622–3634.
11. Katakami R, Sato K, Ogura A. Synthesis of narrow-bandwidth red fluorescent carbon quantum dots for multi-metal ion sensing. *J Mater Chem C.* 2023;11(12):4143–4152.
12. Wu Z, Zhao Y, Zhang N. Green and low-carbon economics: a literature survey using natural experiments. *Green Low Carbon Econ.* 2023;1(1):2–14.
13. Nouri M, Hajiaghababaei L, Badiei A. Chemiluminescence system using $Eu^{3+}/Gd_2O_3@SiO_2$ spheres for quantification of Cr^{6+} ions. *Adv Powder Technol.* 2024;35(9):104595.
14. Kolekar GA, Pawar PS, Gunjal BD. Sulfur-doped carbon dots for selective sensing of Cr^{6+} and Fe^{3+} ions in water samples. *RSC Adv.* 2024;14(5):3473–3479.
15. May BM, Bambo MF, Hosseini SS, Sidwaba U, Nxumalo EN, Mishra AK. I–III–VI ternary quantum dots for fluorescence detection of heavy metal ions in water: a review. *RSC Adv.* 2022;12(18):11216–11232.
16. Meng YT, Jiao Y, Zhang Y, Zhang HL, Gong XJ, Liu Y, et al. One-step synthesis of red-emission carbon dots for detection of berberine and curcumin. *Spectrochim Acta A Mol Biomol Spectrosc.* 2021;251:119432.
17. Yan YN, Zhang HL, Du FF, Meng YT, Shuang SM, Wang RB, et al. N-doped carbon dots for dual-mode detection of curcumin. *Analyst.* 2021;146(17):5357–5361.
18. Liu QS, Dong ZC, Hao AJ, Guo XJ, Dong W. Highly fluorescent carbon dots as a ratiometric probe for detection of chlorogenic acid. *Talanta.* 2021;222:121372.
19. Sistani S, Shekarchizadeh H. Molecularly imprinted polymer-based fluorescence sensor for detection of tannic acid in food samples. *Anal Chim Acta.* 2021;1186:339122.